International Journal of Chemical, Materials and Biomolecular Sciences
ISSN: 2415-6620
Vol:9, No:4, 2015

Multiaxial Fatigue Analysis of a High Performance Nickel-Based Superalloy

P. Selva, B. Lorrain, J. Alexis, A. Seror, A. Longuet, C. Mary, F. Denard

***Abstract*—**Over the past four decades, the fatigue behavior of nickel-based alloys has been widely studied. However, in recent years, significant advances in the fabrication process leading to grain size reduction have been made in order to improve fatigue properties of aircraft turbine discs. Indeed, a change in particle size affects the initiation mode of fatigue cracks as well as the fatigue life of the material. The present study aims to investigate the fatigue behavior of a newly developed nickel-based superalloy under biaxial-planar loading. Low Cycle Fatigue (LCF) tests are performed at different stress ratios so as to study the influence of the multiaxial stress state on the fatigue life of the material. Full-field displacement and strain measurements as well as crack initiation detection are obtained using Digital Image Correlation (DIC) techniques. The aim of this presentation is first to provide an in-depth description of both the experimental set-up and protocol: the multiaxial testing machine, the specific design of the cruciform specimen and performances of the DIC code are introduced. Second, results for sixteen specimens related to different load ratios are presented. Crack detection, strain amplitude and number of cycles to crack initiation vs. triaxial stress ratio for each loading case are given. Third, from fractographic investigations by scanning electron microscopy it is found that the mechanism of fatigue crack initiation does not depend on the triaxial stress ratio and that most fatigue cracks initiate from subsurface carbides.

***Keywords*—**Cruciform specimen, multiaxial fatigue, Nickel-based superalloy.

I. Introduction

INCONEL 718 has been predominantly used in aeronautic engine components, such as turbine discs and shafts, as they combine high temperature strength, toughness, good creep and rupture strengths as well as good corrosion endurance.

Over the past four decades, extensive investigations on the fatigue life of Inconel 718 have been made, such as the effect of temperature on the cyclic strain-stress response [1], the mechanism-based modeling of fatigue life prediction [2], the fatigue behavior up to the very high cycle regime [3] and so on.

In recent years, significant advances in the fabrication process of Inconel 718 leading to grain size reduction have been made in order to improve fatigue properties of aircraft turbine discs. A change in grain size affects the initiation mode of fatigue cracks as well as the fatigue life of the material [2], [4]. Indeed, fine grain size generally provides better fatigue resistance than coarser grains as more grain boundaries aid in transcrystalline crack arrest and thus reduce fatigue crack growth rates. However, if grains size is reduced down to primary carbides dimensions, the latter may act as fatigue crack initiation sites and involve premature failures. Therefore, experimental data are ultimately needed so as to investigate and to assess the fatigue life of this new developed superalloy.

In order to get results in conditions representative of the one encountered in most service conditions, biaxial-planar fatigue tests are performed at different stress ratio on cross shaped specimens. Experiments are carried out at different stress ratios in order to study the influence of the multiaxial stress state on the fatigue life of the material.

First, the design of the specimen as well as the experimental setup and procedure are presented. Second, low cycle fatigue tests are carried out at room temperature on a biaxial-planar servo-hydraulic tension-compression testing machine at different stress ratios. Full-field displacement and strain measurements as well as crack initiation detection are obtained using Digital Image Correlation techniques. Finally, fracture surfaces are investigated using scanning electron microscopy in attempt to determine the origin/cause of failure.

II. Test Specimen Design

Various designs of cruciform specimens have been investigated in attempt to obtain the maximum of deformation at the center of the specimen and at the same time to avoid stress concentrations in other regions [5]. For instance, reduced section type specimens were studied by [6]-[8]; [9] used specimens containing a series of slits in its arms, while [10] combined both characteristics. However, no standard geometry exists.

In the present study, cruciform Inconel 718 specimens with a reduced section in the gauge zone are utilized (Fig. 1). Note that for confidential reasons most dimensions of the specimen as well as chemical composition, microstructure and material properties are not revealed.

Based on the design proposed by [11], the geometry has been further optimized using numerical simulations so as to produce a stress and strain concentration with homogenous distribution in the central part, to increase the stress deviation between the gauge area and the specimen arms, and to maximize the stressed volume in the gauge zone.

P. S. is with the Centre d'Ingénierie en Mécanique, Matériaux et Surfaces, ENIT, 65016 Tarbes, France (corresponding author to provide phone: 0033-562-442-932; fax: 0033-562-445-087; e-mail: pierre.selva@enit.fr).

B.L. and J.A. are with Université de Toulouse, LGP, ENIT/INPT, 65016 Tarbes, France (e-mail: b.lorrain@enit.fr; j.alexis@enit.fr).

A.S., A.L., C.M., and F.D. are with Safran-Snecma, Direction Technique, Etablissement de Villaroche, 77550 Moissy-Cramayel, France (e-mail: alexandre.seror@snecma.fr).

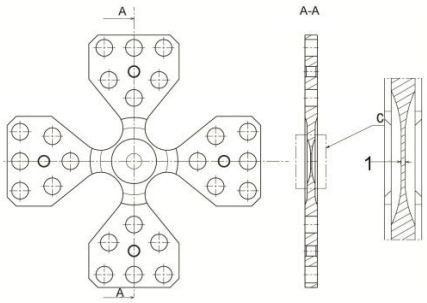

Fig. 1 Visualization of the von Mises stress

For the worst case of loading investigated hereafter (equibiaxial tension at 95 kN), finite element (FE) simulations were performed using the commercial FE Abaqus 6.10 software [12]. Briefly, the FE model considers one eighth of the specimen for symmetry reasons. A three-dimensional mesh (Fig. 2) is generated using 11550 20-nodes quadratic brick elements (element C3D20R in Abaqus). Symmetry plane boundary conditions are set up along the $\langle X,Y\rangle$, $\langle Y,Z\rangle$, and $\langle X,Z\rangle$ planes, and pressure load is applied at each arm extremity. An elasto-plastic behavior combined with a nonlinear kinematic hardening model with two backstresses is considered.

Fig. 2 shows the von Mises stress field for a 95 kN biaxial tensile loading applied to three different designs: the initial geometry having a central thickness of 1.6 mm, a second geometry with a reduced thickness of 1 mm in the gauge zone, and an optimized design considering a central thickness of 1 mm along with an increase of the triple fillet radius at the intersection of two arms. This final design reduces the stress in the arms to 90% of the maximum von Mises stress. This maximum is located in the gauge zone where the stress distribution is uniform.

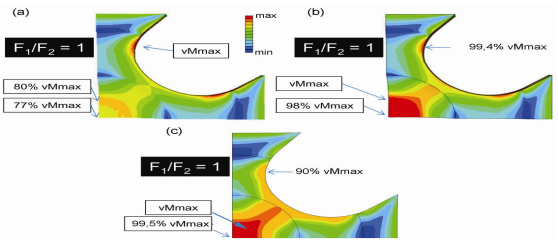

Fig. 2 Visualization of the von Mises stress field for an equibiaxial loading of 95 kN applied to three different designs. (a) Initial design with a central thickness of 1.6mm; (b) Second design with a reduced thickness of 1mm in the central part; (c) Optimized design with a central thickness of 1 mm and modified fillet radius

It is worth mentioning that, right after the manufacturing process; topographical characterization of the central zone of the specimens is performed using optical profilometry. Indeed, a very high proportion of all fatigue failures nucleate at the surface of components and so surface conditions constitute an extremely important factor influencing fatigue strength. In the present study, a fine polished finish of 0.2 micron maximum Ra value (roughness average defined by the absolute value of the surface height averaged over the surface) is obtained in this region.

III. Experimental Set-up

A. Biaxial Testing System

Fatigue tests are performed on the Instron biaxial cruciform testing system of the ENIT laboratory (Fig. 3). The cruciform load frame is a rigid structure comprising a support base and an octagonal frame incorporating four 100kN hydraulic actuators. These actuators equipped with hydrostatic bearings have a ±20mm stroke range and are rated for operation at 280 bar supply pressure. The testing machine uses a digital controller to provide translation and deformation control of each axis. Each actuator may be operated in either non-modal control – which means actuators are controlled independently - or in modal control – which means that both actuators along the same axis are controlled dependently. In the latter case, closed-loop control using linear combinations of the two forces F_1 and F_2 and of the two displacements u_1 and u_2 of two opposite actuators is performed. In the present case, the mean force $(F_1+F_2)/2$ and mean displacement $(u_1+u_2)/2$ as well as the force difference $(F_1-F_2)/2$ and the displacement difference $(u_1-u_2)/2$ are implemented to control each axis. This permits, first, to avoid specimen center-point floating which could induce bending in the specimen resulting in an uncontrolled stress state and second, to avoid significant side loads which are detrimental to the actuators. The center of the specimen can also be considered as motionless throughout the test.

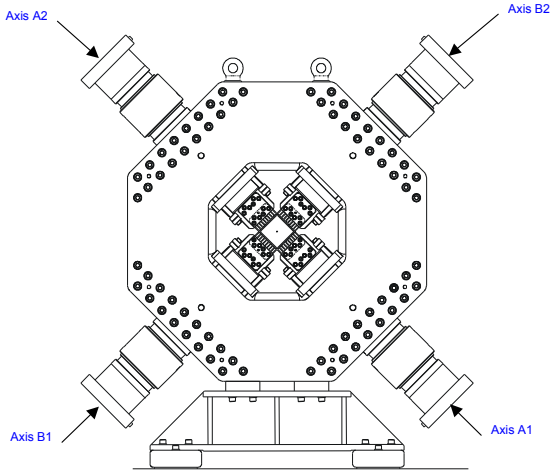

Fig. 3 Visualization of the biaxial testing machine

B. Loading Conditions

Through the literature, biaxial loading conditions are commonly derived from te desired biaxial stress ratio defined by $b=\sigma_2/\sigma_1$ when $|\sigma_2/\sigma_1|<1$ or $b=\sigma_1/\sigma_2$, with $|\sigma_3|\ll(|\sigma_1|,|\sigma_2|)$, where $(\sigma_1,\sigma_2,\sigma_3)$ are the principal stresses. However, this ratio could be confusing as two different loading paths could provide the same value of b. For instance, equibiaxial compression-compression and tension-tension tests provide the same biaxial stress ratio of 1. In the

following, we rather consider a triaxial stress ratio T defined by the ratio of the first invariant of the stress tensor and the equivalent von Mises stress such as:

$$T = \frac{Tr(\sigma)}{\sigma_{VM}} \quad (1)$$

Considering that $|\sigma_3| \ll (|\sigma_1|, |\sigma_2|)$ then the relation between b and T is straightforward:

$$T = \pm \frac{1+b}{\sqrt{1-b+b^2}} \quad (2)$$

Specimens are subjected to a 1 Hz sinusoidal cyclic loading. In order to study the influence of the multiaxial stress state on the fatigue life, four different loading paths are considered: one proportional equibiaxial test in tension-tension cyclic loading at 95 kN, one proportional test in tension-tension cyclic loading equivalent to a compensated uniaxial test ($T = 1$), one proportional tests in tension-tension cyclic loading producing a triaxial stress ratio of 1.73, and one proportional test in tension-compression producing a triaxial stress ratio of 0.48. Forces required and provided by each actuator to obtain a specific value of triaxial stress ratio are computed from finite element simulations (Fig. 4). It should be noted that the different multiaxial loading paths share the same maximum von Mises equivalent stress σ_{VM}^{max} .

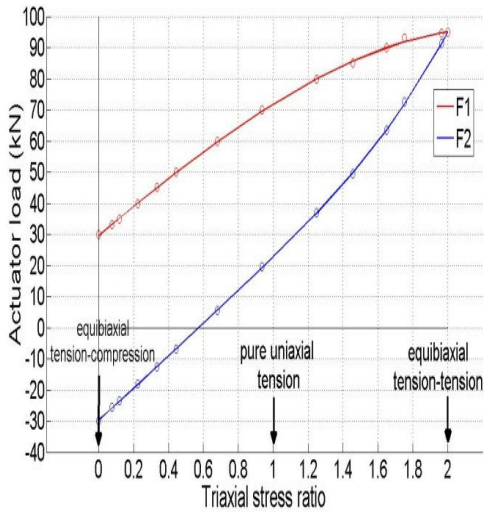

Fig. 4 Plot of the actuator loading as a function of triaxial stress ratio

Table I summarizes the different loading paths used in the present study. They all consider a load ratio $R_F=F_{min}/F_{max}=0.05$.

TABLE I
DEFINITION OF THE LOADING PATHS

Test	Triaxial stress ratio	$(F_x^{min}\|F_x^{max})$	$(F_y^{min}\|F_y^{max})$
1	T=0.48	(-5|-0.25)	(2.55|51)
2	T=1	(1.15|23)	(3.6|72)
3	T=1.73	(3|60)	(4.45|89)
4	T=2	(4.75|95)	(4.75|95)

C. Instrumentation

The specimens are instrumented with strain gauges in order to ensure that no flexion is induced when positioning them into the testing machine and during the test. Strain measurements are recorded using a multichannel data acquisition system until the gauges come off.

Two high-speed cameras (Phoron Fastcam SA61.1) capable of recording 50 frames per second at megapixel resolution (1024x1024 pixels) are set up, one facing each side of the specimen. A data acquisition module (National Instrument 6211) is used to synchronize image acquisitions with the load signal of the fatigue testing machine. The filtering of the command signal induces a delay of 8 ms to trigger both cameras. The acquisition sequence, which consists of recording 50 images during one cycle at different period of time, is as follows:

- From cycle 1 to 10 : every cycles
- From cycle 100 to 1000 : 1 cycle over 100
- From cycle 2000 to 10000 : 1 cycle over 1000
- From cycle 10100 till the rupture of the specimen: 1 cycle over 100.

After the completion of testing, digital image correlation is performed using the commercial Aramis software [13]. This optical full-field measurement technique allows studying qualitatively as well as quantitatively the mechanical behavior of materials. Typically, the surface displacements are first measured with DIC. Strains are subsequently calculated by numerical differentiation of the measured displacement field.

D. DIC Performance

Prior to any test, performances of the DIC algorithm are evaluated. To perform DIC a random speckle pattern, which is handily performed by spray painting, is applied on both sides of the specimens. From a speckle-pattern reference image, two sets of images are artificially constructed with Fast Fourier Transformation. A sub-pixel displacement field is applied to the first set of images while a strain field is prescribed to the second set. Using these data as input, performances of the image processing algorithm are assessed by comparing the correlation software outputs with the exact imposed values. Errors are then statistically analyzed in terms of systematic error (mean difference between the measured and the prescribed fields) and uncertainty (standard deviation of the measured field). Note that calculations are performed on a regular $N \times N$ square grid with no overlap.

In the present case, the mean error is always under 4.2×10^{-3} pixel equivalent to 0.075 µm. The measurement uncertainty in displacement clearly depends on the mesh size. A value of 0.027 pixel is obtained with a mesh size of 10×10 pixels while an uncertainty of 0.011 pixel is computed if square subsets of 20 pixels are used. However, beyond a mesh size of 20×20 pixels, the gain on uncertainty is poor but there is a decrease in spatial resolution.

A similar analysis is made on the strain field. From a grid size of 20 pixels the strain uncertainty exhibits similar values, around 0.019 %. The systematic error strongly depends on the prescribed strain value. FE simulations predict a maximum

strain in the gauge zone of about 1%. This corresponds to a systematic error of 0.012%. We also note that the systematic error is not affected by the mesh size.

For the actual tests a subset size of 20 pixels is used. This represents a fair compromise between measurement error and uncertainty, spatial resolution and computation time.

IV. Experimental Results

A. Crack Initiation Detection and Fatigue Lives

In the present study, DIC is used to determine the number of cycles to crack initiation and not to analyze crack propagation. As already mentioned, the experimental set-up allows performing DIC on both sides of the specimens.

For the sake of comparison, we chose to plot the equivalent von Mises strain field ε_{VM} for all the tests performed with different biaxial loading types. Fig. 5 gathers the following test results according to each load case: maximum force F^{max}, triaxial stress ratio T, von Mises strain field ε_{VM} plotted on the front side of the specimen at N=10 cycles, von Mises strain field plotted at crack initiation and the displacement field at crack opening. Each test considers a load ratio ratio $R_F=F_{min}/F_{max}=0.05$. Plots of ε_{VM} at N=10 clearly show that the strain field exposes a fairly symmetrical pattern, which means that the actual load is uniformly distributed. Prior to crack opening, crack initiation location is first detected by a local strain gradient, which is due to local plasticity, either on the front or back side of the specimen. We can observe that crack initiation occurs either in the gauge zone or in the transition area due to the notch effect of the radius. After a few hundreds cycles, the crack opens and a discontinuity is observed in the displacement field computed from DIC.

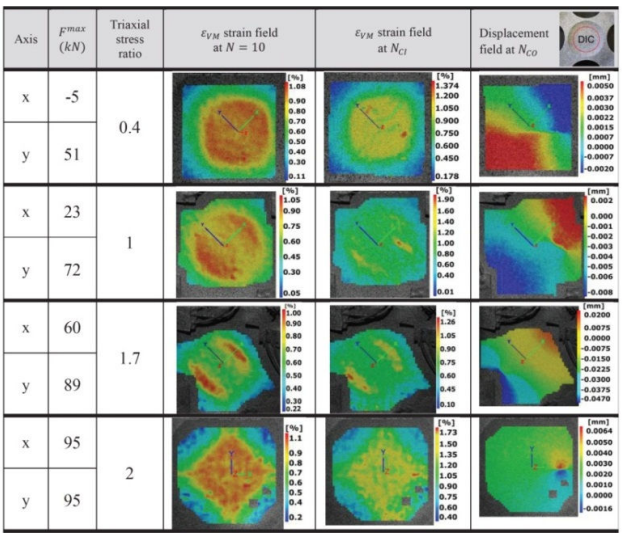

Fig. 5 Test results. Plots of the equivalent von Mises strain field at the beginning of each test (N=10), at crack initiation (N=N_{ci}) and plot of the displacement field at crack opening (N=N_{co})

The first appearance of the crack, which cannot be seen with the naked eyes and the number of cycles to crack initiation are precisely determined as images are recorded every 100 cycles. The triaxial stress ratio versus numbers of cycles to crack initiation is plotted in Fig. 6. Mean values are represented by dots while the standard deviation is represented by vertical lines. The number of cycles has been normalized with respect to the mean value of N derived from compensated uniaxial tests ($T = 1$). Fig. 5 clearly shows the influence of the multiaxial stress state on the fatigue life of the material. For a triaxial stress ratio within the range [1.7 - 2] the number of cycles to crack initiation is similar and lower than in the case of a compensated uniaxial test ($T = 1$). On the contrary, fatigue life is significantly extended for triaxial stress ratio lower than 1, especially when compression is part of the loading path.

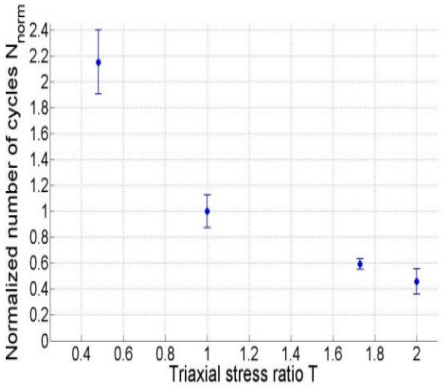

Fig. 6 Evolution of the normalized number of cycles to crack initiation with respect to the triaxial stress ratio. Mean points) and standard deviation (error bars) are plotted

For the sake of comparison, we chose to plot the equivalent von Mises strain field ε_{VM} for all the tests performed with different biaxial loading types.

B. Fractographic Investigation

All tested specimens are subjected to fractographic investigation by macrographic examinations, light microscope and scanning electron microscope (SEM). First, macroscopic crack orientations within the specimens are investigated (Fig. 7). For the equibiaxial tests the macroscopic crack growth occurs under about 45° to the loading axes in mode I. Both triaxial stress ratios of 1 and 1.73 produce crack growth also in mode I but in a plane perpendicular to the direction of the main principal stress. When compression loading is introduced (triaxial stress ratio of 0.48), the crack front is no longer a straight line and propagates with a zig-zag path as the fatigue crack growth occurs in a mixed mode (I+II). Second, from macrographic examinations of each rupture facies, i.e. by visual examination or by low-magnifications optical microscopy, crack initiation sites and crack propagation through thickness are clearly identified (Fig. 8). For all the tests, cracks originate from surface locations and propagate throughout the thickness of the specimen.

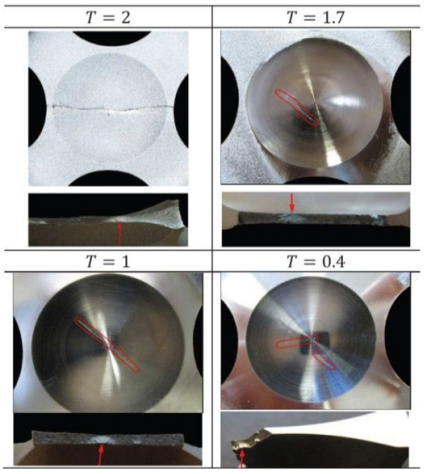

Fig. 7 Crack orientation within the cruciform specimen in respect to different stress state (triaxial stress ratio T) and macrographic observation of each rupture facies where crack propagation is clearly visible

Investigations of the fracture surfaces are then completed using SEM, in particular at crack origins (stage I) and in the zone of crack propagation (stage II). Elemental mappings on crack initiation sites are also obtained using Energy Dispersive X-ray Spectroscopy (EDS). In all tests, SEM observations of fracture surfaces revealed crack initiation sites with a faceted-crystallographic aspect. Some quasi-cleavage facets [14] were also observed in specimens, but not in a large numbers. Crack origins were found to be primary carbides cluster which are located within the surface layer of the specimen (Fig. 9). Cracked carbides of dimensions equivalent to the grain size are clearly shown in Fig. 8.

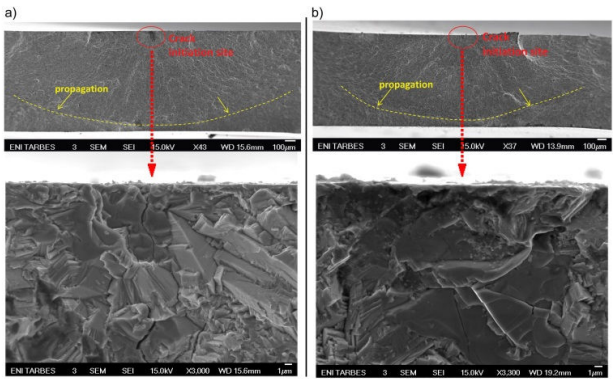

Fig. 8 SEM observations of crack propagation and cracked carbides on rupture facies of cruciform specimens under in-plane biaxial cyclic loading. a) proportional equibiaxial tension-tension test at 95 kN; b) proportional tension-tension test at 60 kN / 89 kN

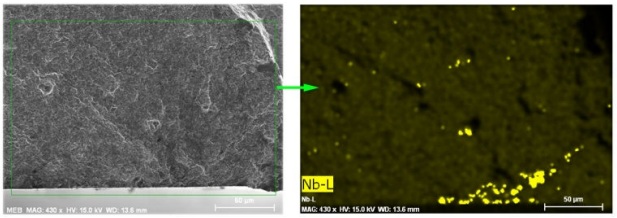

Fig. 9 Example of niobium mapping on crack initiation site obtained using Energy Dispersive X-ray Spectroscopy (EDS). A cluster of niobium carbides is clearly visible

Regarding tension-compression tests, smeared surface structures showing signs of oxidation were frequently observed (Fig. 10). This can be explained by the shear stress component involving the friction of opposing fracture surfaces. This phenomenon greatly complicates the exact crack location determination. While tension-tension tests produce cracks that propagate radially throughout the thickness of the specimens (Fig. 8), crack growth is considered to spread out elliptically by mode II shear in the case of tension-compression tests (Fig. 10).

Finally, for every test conditions, typical fatigue striations of about 1 µm oriented perpendicular to the microscopic direction of crack propagation are revealed in the stage II area.

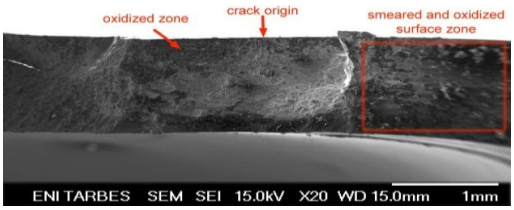

Fig. 10 SEM observation of a rupture facies in the case of a tension-compression test (T=0.48). Smeared surface structures and oxidized zones (dark zones) are observed. Crack initiates from subsurface carbides and spread out elliptically through the thickness of the specimen

V. Conclusion

A large experimental campaign at room temperature to study the biaxial-planar low cycle fatigue behavior of a newly developed nickel-based superalloy is performed.

Different stress ratios are considered and all tests share the same maximum von Mises equivalent stress. In each case, location of the first crack has been detected from DIC either on the front or back side of the specimens. The relationship between the level of stress ratio and the number of cycle to crack initiation has been clearly identified. The lower the triaxial stress ratio, the longer is the fatigue life of the material. In particular, fatigue life is significantly extended for triaxial stress ratio lower than 1 (compensated uniaxial test), especially when compression is part of the loading path.

Finally, fractographic investigations have revealed that, first, cracks originate from surface locations and propagate throughout the thickness of the specimen and, second, that carbides or cluster of carbides may act as nucleation sites for fatigue cracks. It seems that, for the level of σ_{VM}^{max} tested in the

present study, the mechanism of fatigue crack initiation does not depend on the triaxial stress ratio. Thus the fatigue life of the material is directly related to the level of the multiaxial stress state.

ACKNOWLEDGMENT

The authors thank C. O'Keeffe for relevant advices and helpful comments on the manuscript.

REFERENCES

[1] D. Fournier, A. Pineau, "Low cycle fatigue behavior of Inconel 718 at 298K and 823K", Metallurgical Transactions A, vol. 8A, pp. 1095-1105, 1977.
[2] F. Alexandre, S. Deyber, A. Pineau, "Modelling the optimum grain size on the low cycle fatigue life of a Ni based superalloy in the presence of two possible crack initiation sites", Scripta Materialia, vol. 50, pp. 25-30, 2004.
[3] X.F. Ma, Z. Duan, H.J. Shi, R. Murai, E. Yanagisawa, "Fatigue and fracture behavior of nickel-based superalloy Inconel 718 up to the very high cycle regime", Journal of Zhejiang Univ-Sci – Applied Physics & Engineering, vol. 10, pp. 727-737, 2010.
[4] V. Zerrouki, "*Inconel 718 et tenue en fatigue oligocyclique. Influence de la microstructure et prédiction de la durée de vie*", Mémoire de DRT Génie des Matériaux, Université EVE, 2000.
[5] Y. Ohtake, S. Rokugawa, H. Masumoto, "Geometry determination of cruciform type specimen and biaxial tensile test of C/C composites", Key Eng. Mater., vol. 3, pp. 151-154, 1999.
[6] S.B. Lin, J.L. Ding, H.M. Zbib, "Characterization of yield surfaces using balanced biaxial tests of cruciform plate specimens", Scripta Metall. Mater., vol. 28, pp. 617-622, 1993.
[7] J.S. Welsh, D.F. Adams, "An experimental investigation of the biaxial strength of IM6/3501-6 carbon /epoxy cross-ply laminates using cruciform specimens", Composites: Part A 33, vol. 6, pp. 829-839, 2002.
[8] M. Poncelet, G. Barbier, B. Raka, S. Courtin, R. Desmorat, J.C. Le-Roux, L. Vincent, "Biaxial high cycle fatigue of a type 304L stainless steel: cyclic strains end crack initiation detection by digital image correlation", European Journal of Mechanics / A Solids, vol. 5, 2010.
[9] P. Terriault, K. Settouane, V. Brailovski, "Biaxial testing at different temperatures of cruciform Ti-Ni samples. In: Shape Memory and Superelastic Technologies", California, 2003.
[10] A. Makinde, L. Thibodeau, K.W. Neale, "Development of an apparatus for biaxial testing for cruciform specimens", Experimental mechanics, vol. 32, pp. 132-137, 1992.
[11] A. Scholz, C. Berger, A. Samir, R. Bardenheier, "Biaxiale TMF-Simulation mit Kreuzproben zur Untersuchung des Kriechermüdungsverhaltens von hochtemperaturewerkstoffen. Weinheim", Wiley, pp. 280-285, 2007.
[12] Abaqus Analysis User's Manual v6.10.
[13] Aramis software. Gom Optical Measuring Techniques. http://www.gom.com/EN/index.html, 2006.
[14] S.P. Lynch, "Progression markings, striations, and crack-arrest markings on fracture surfaces", Materials Sciences and Engineering A, 468-470, pp. 74-80, 2007.